Aeroacoustics Conferences
20-23 May 2019, Delft, The Netherlands
25th AIAA/CEAS Aeroacoustics Conference

10.2514/6.2019-2664

Crackle-related beamforming of military jet aircraft noise

Aaron B. Vaughn,[1] Kent L. Gee,[2] S. Hales Swift,[3] Kevin M. Leete,[4]
Brigham Young University, Provo, UT, 84602

Alan T. Wall,[5]
Air Force Research Laboratory, Wright-Patterson Air Force Base, OH, 45433

and

J. Micah Downing,[6] Michael M. James[7]
Blue Ridge Research and Consulting, LLC, Asheville, NC, 28801

Crackle is a perceptual feature of supersonic jet noise that is related to the presence of acoustic shocks. This study investigates the apparent source locations of events related to crackle for a high-performance military jet aircraft using an event-based, time-domain beamforming method. This method utilizes the cross correlation between adjacent microphones to determine the angle of propagation of an ensemble of shock-related events within the time waveform. This angle of propagation is then traced back towards the source to find the apparent source location. Based on the angle of propagation, derivative skewness, and overall sound pressure level, the microphone pairs along the array can be sorted into six groups. With increasing engine condition, groups related to the presence of crackle tend to shift downstream and broaden, in qualitative agreement with the general aeroacoustic source locations. However, a comparison with near-field acoustical holography shows that the apparent source region of crackle-related events appears upstream of the overall energy at intermediate power but appear to converge at maximum afterburner.

Nomenclature

BBSAN	=	broadband shock-associated noise
D	=	nozzle diameter, m
dSk	=	skewness of pressure time derivative, “derivative skewness”
ETR	=	engine thrust request
MARP	=	measurement array reference point
NAH	=	near field acoustical holography
OASPL	=	overall sound pressure level, dB
PDF	=	probability density function
SPL	=	sound pressure level, Pa
x	=	sideline distance, m
z	=	axial distance, m
$\Delta\tau$	=	cross-correlation time lag, s
θ	=	polar angle from engine inlet, degrees
ϕ	=	offset angle of the microphone array from the jet centerline, degrees
ψ	=	incident angle to the microphone array, degrees

[1] Graduate Student, Dept. of Physics and Astronomy, N283 ESC.
[2] Professor, Dept. of Physics and Astronomy, N243 ESC, AIAA Senior Member.
[3] Postdoctoral Research Associate, Dept. of Physics and Astronomy, N283 ESC, AIAA Member.
[4] Graduate Student, Dept. of Physics and Astronomy, N283 ESC.
[5] Research Physicist, Battlespace Acoustics Branch, Air Force Research Laboratory, 2610 Seventh St., Bldg. 441, Wright-Patterson AFB, OH 45433, AIAA Member, AIAA Member.
[6] Senior Scientist, 29 N Market St, Suite 700, AIAA Member.
[7] Senior Principal Engineer, 29 N Market St, Suite 700, AIAA Member.

I. Introduction

Crackle is an audible component of high-power jet noise that has been called both annoying[1] and dominant.[2] Ffowcs Williams *et al.*'s[1] initial study of crackle in supersonic commercial aircraft noise described these aircraft as "particularly prone to producing sudden spasmodic bursts of a rasping fricative sound." They further stated, "It is a startling staccato of cracks and bangs and its onomatope, 'crackle' conveys a subjectively accurate impression." Since the publication of the initial investigation, differing metrics, models, and methodologies for study have emerged in the jet noise literature. For this paper, we define crackle as a perceptual feature of supersonic jet noise that is related to the reception of acoustic shocks. This is in accord with Ffowcs Williams *et al.*'s assertion that the "physical feature of a sound wave that gives rise to the readily identifiable subjective impression of 'crackle' is shown to be the sharp shock-like compressive waves that sometimes occur in the waveform."[1]

Acoustic shocks are rapid pressure increases that are characterized by large positive pressure derivatives. For supersonic jet noise, nonlinear effects cause the formation, strengthening, and persistence of these shocks in the far field.[3-7] Although the far-field shock evolution is of importance to quantifying community response to flyovers at high powers, source-related investigations are also of importance because of the potential to understand and optimize noise reduction methods and technologies, such as those described in Refs. 8 and 9. This paper reports results of an investigation to study the origins of acoustic shocks received in the geometric near field of a military jet aircraft and to connect these results with recent studies of the crackle percept.

A growing number of investigations of crackle or acoustic shock-related studies have used diverse jet conditions, scales, measurement or simulation methods, analysis techniques, and criteria.[7, 10-19] In these various studies, different conclusions have been reached regarding the presence of steepened-wave or shock-like features in the jet and their subsequent propagation. Unlike all prior studies of crackle, this paper introduces an analysis approach founded on a crackle criterion that has been rigorously tied to human subject testing.[20-23]

Prior studies[20,21] utilized signal processing and informal listening tests to identify the skewness of the time-derivative of the pressure waveform, or derivative skewness (dSk), as a measure for the crackle percept. Recently, a relationship between derivative skewness and crackle has been quantified in the first formal, jury-based listening study of crackle.[22,23] The study employed F-35A waveforms with various degrees of crackliness and a range of values of both pressure skewness (the foundation for the original Ffowcs Williams *et al.*[1] criterion) and derivative skewness. A total of 31 participants auralized the waveforms as part of a category subdivision scaling test and also rank-ordered them in a complementary exercise. The subdivision scaling test resulted in a model for five crackliness categories (smooth noise, rough noise, intermittent crackle, continuous crackle, intense crackle) based on derivative skewness, whereas the relationship between pressure skewness and the crackle percept was found to be statistically insignificant. The listening test revealed that dSk > 3 indicated that "continuous crackle" was present in a jet noise waveform. This criterion is used as part of the analysis reported herein.

To find the regions in the jet responsible for crackle-containing waveforms in the field, this study examines the origins of waveform segments chosen by the presence of large positive derivatives. The origins of these waveform segments are calculated by a two-point cross-correlation beamforming method. A brief summary of the acoustical measurement of the F-35B high-performance military aircraft is provided, followed by a description of the methodology used in the beamforming process. Results for four engine conditions are then discussed, which are followed by a brief comparison with near-field acoustical holography results.

II. Measurement

Acoustic pressure waveforms were collected from a static F-35B operating at several engine conditions, from 25% to 150% engine thrust request, ETR. Engine conditions greater than 100% ETR are due to the addition of afterburner. Although a much more extensive measurement array was present,[24] this paper focuses on data acquired from a 71-element, linear ground array. This array, which was located approximately 8-10 m from the jet estimated shear layer, is shown in Fig. 1. It consisted of GRAS 6.35 mm (1/4") Type 1 microphones which spanned 32 m with a 0.45 m (18 in) inter-microphone spacing. The pressure waveforms were synchronously acquired with National Instruments PXI-449X cards sampling at 204.8 kHz. Time waveforms were at least 27 s long for all engine conditions except for 130% ETR, which only had 10 s. Jet inlet angles were defined for each microphone location relative to the microphone array reference point (MARP), which was set to approximately 7.5 D downstream of the nozzle exit plane to be consistent with prior measurements. Other analyses of this array are reported on in Refs. 25-30.

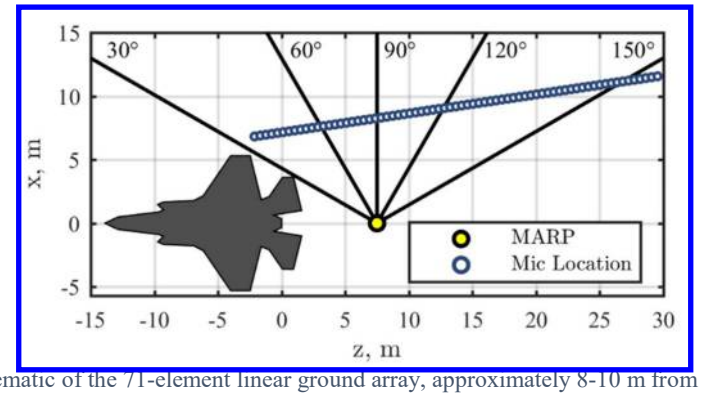

Figure 1. Measurement schematic of the 71-element linear ground array, approximately 8-10 m from the estimated jet shear layer. Inlet angles are defined relative to the microphone array reference point (MARP).

III. Methods

This paper employs an event-based beamforming method involving a cross correlation of adjacent microphones' waveforms windowed around particular events, from which the radiation angle and apparent origin of the events are calculated. The analysis method, which builds off of that described by Vaughn *et al*. in Ref [30], also resembles the method used by Schlinker *et al*.[31,32] to detect the apparent acoustic origins along the jet axis of large-amplitude events for both laboratory and full-scale jets. A previous study by Vaughn *et al*.[30] examined three types of event triggers: maximum pressure values (similar to Schlinker *et al*.), maximum derivative values, and regularly-spaced, non-overlapping waveform segments. However, only the maximum derivative events are considered in the present analysis, for two reasons. First, the three types of event definitions revealed similar source characteristics, as high-amplitude events were correlated with high-derivative events and even relatively short event windows typically contained a high-derivative or high-amplitude event within the regularly spaced segments. Second, the large derivative values are directly linked to elevated derivative skewness, which in turn is directly correlated with the crackle percept as quantified by Gee *et al*.[22,23] The relation between the large-derivative event trigger and derivative skewness are elaborated in the following section.

A. Event Selection Method

Short F-35B waveform segments with and without acoustic shocks are shown in Fig. 2. The waveform in Fig. 2a has a more random nature to it, whereas the waveform in Fig. 2b has distinct acoustic shocks present characterized by sudden pressure increases followed by rarefactions of longer durations. Corresponding derivatives of these waveforms are presented in Figs. 2c and 2d. Peaks in these plots correspond to sudden increases in pressure, or acoustic shocks. Based on the Gee *et al.*[22] crackle criteria, the waveform represented by the segment in Fig. 2a (dSk = 0.6) is considered to not contain crackle and the waveform represented in Fig. 2b (dSk = 9.4) would contain "intense crackle."

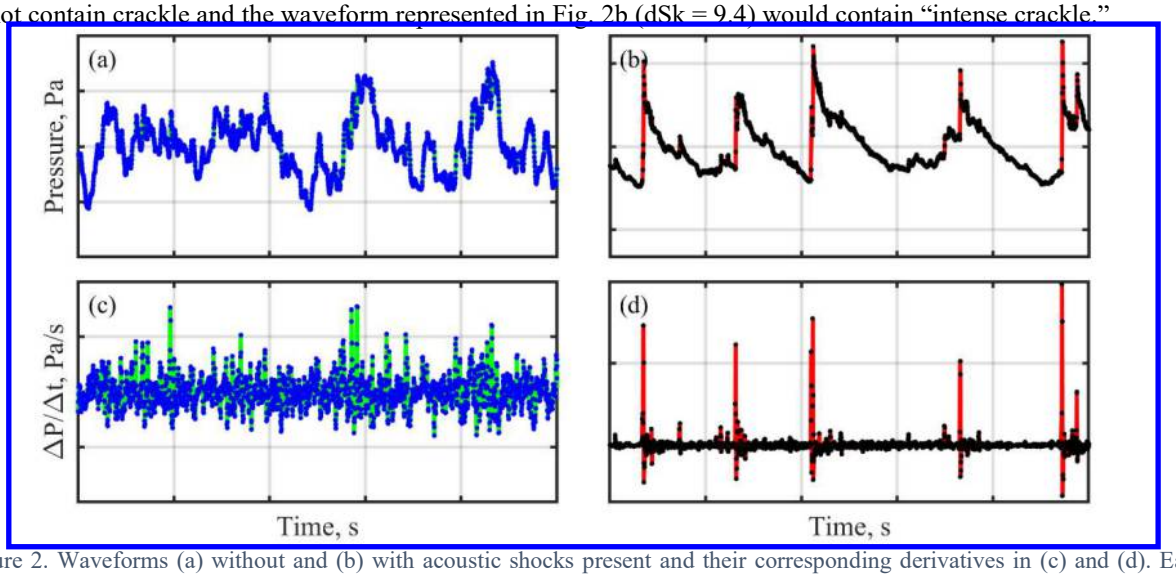

Figure 2. Waveforms (a) without and (b) with acoustic shocks present and their corresponding derivatives in (c) and (d). Each waveform is 10-ms in length and from 150% ETR with the microphone location of (a) and (c) at the farthest upstream location (z = -2.1 m) along the array shown in Fig. 1 and (b) and (d) towards the maximum radiation region (z = 11 m).

Crackle has been shown to be highly correlated with derivative skewness, yet the aim here is to use high derivatives to trigger the event-based beamforming approach. The relationship between the pressure derivative, $\Delta p/\Delta t$, and the derivative skewness, dSk, is shown in Fig. 3 with the time-derivative of a 10-s pressure waveform in blue, the running dSk value calculated for non-overlapping 20-ms segments in red, and the time-averaged derivative skewness value of 3.6 in green. Large peaks in the time-derivative of the pressure waveform represent high-derivative events, and the largest derivative skewness values occurring simultaneously with these peaks, indicating that these events contribute most significantly to the overall derivative skewness value of the waveform. Using this direct link of dSk with the large-derivative events in conjunction with the result of the prior subjective studies,[22,23] the maximum derivative events are used in the subsequently described event-based beamforming method.

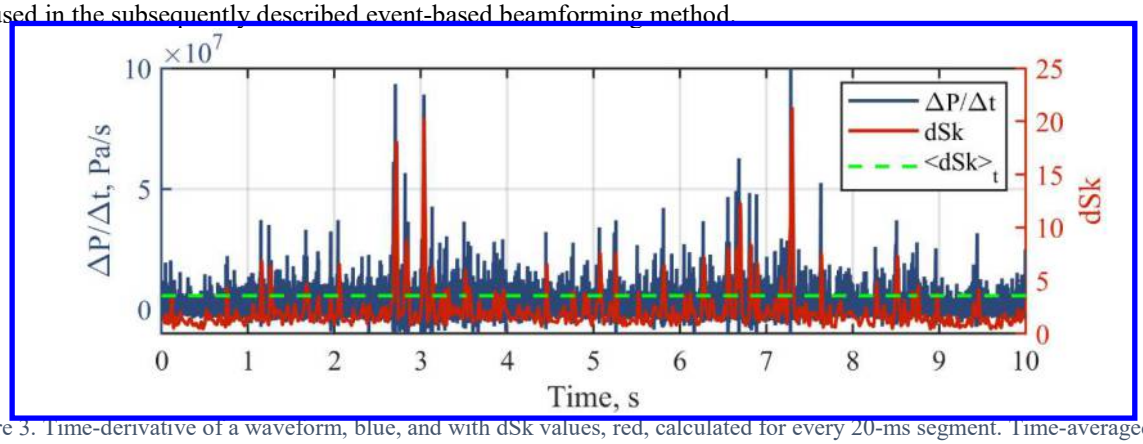

Figure 3. Time-derivative of a waveform, blue, and with dSk values, red, calculated for every 20-ms segment. Time-averaged dSk is indicated by the green dashed line.

B. Beamforming Method

A two-point cross-correlation beamforming method is used to find the apparent propagation angles and source locations of the events defined in the previous section. For every pair of adjacent microphones along the array, the events are selected in the upstream microphone. In the 27-s waveforms, the derivative values were sorted in descending order, and the top one thousand were selected with the condition that they were not within 2.4 ms of each other. An example of a defined event is indicated by the red x in Fig. 4a. Events defined in the reference channel may or may not become events in the adjacent channel when the adjacent channel is used as a reference channel for the next microphone pair, as this depends upon a given large derivative persisting across multiple microphones. For example, the acoustic shock that occurs at about 8.5-ms in the reference channel in Fig. 4a is seen as having a significantly reduced amplitude at about 9-ms in the adjacent channel in Fig. 4b. Fievet *et al.*[14] observed that not all waves propagate in the same direction with the possibility of crossing waves, however, further investigation is needed to understand why particular acoustics shocks change drastically between adjacent microphones.

After events are defined, a window is applied around each event in both the reference and adjacent channels, as shown in Fig. 4. The window is centered about the defined event in the reference channel, but when applied to the other channel in the pair a lag is applied. This time lag is determined by assuming the MARP as the source and determining the relative time lag due to their relative distances to the MARP. The window is a 20-ms Hann function which was chosen to be sufficiently long that if the event in the adjacent channel does not line up in the center of the window, there is still enough information in the corresponding event to compute a meaningful cross correlation. Due to the length of the window, two events may overlap. However, most (>90%) events occur at least 5-ms from the next closest event, where the window drops by 50%, so most of the information captured by the different waveform segments can be considered independent of the others.

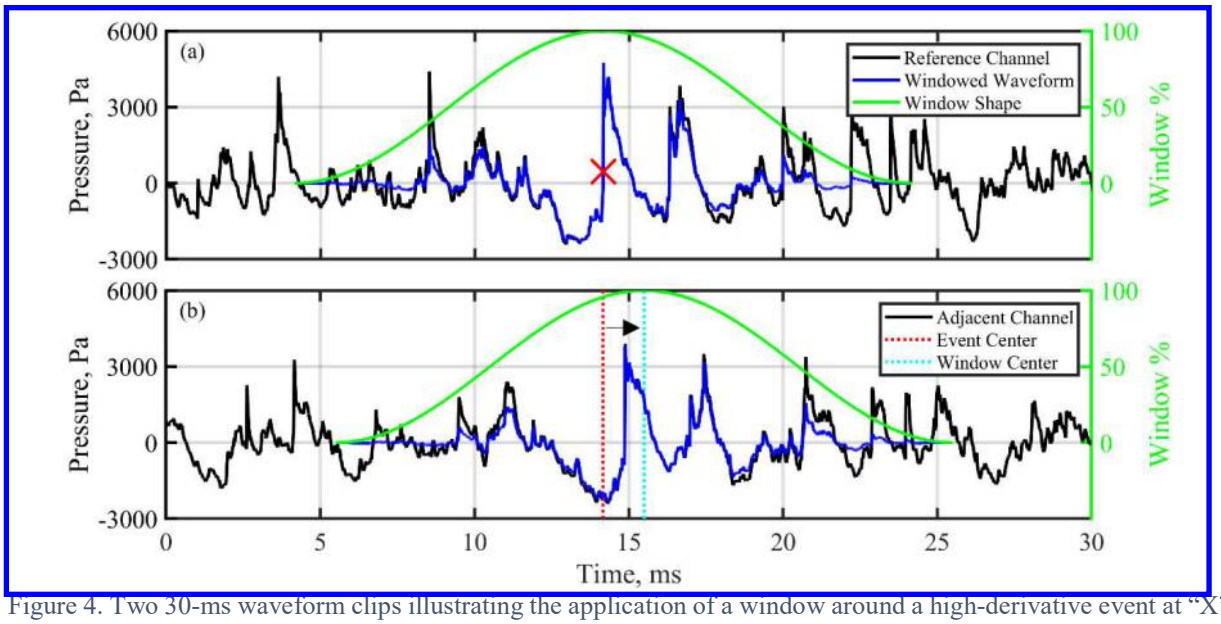

Figure 4. Two 30-ms waveform clips illustrating the application of a window around a high-derivative event at "X" in (a) the reference channel and (b) the adjacent channel. Solid black line indicate the unaltered waveform, blue the windowed waveform, green the window shape. Dashed red line indicates the time at which the event occurs in the reference channel and the dashed cyan line is where the time-shifted window is centered in the adjacent channel.

To obtain the apparent origin for each windowed waveform, a two-microphone cross-correlation method is used as a time-domain beamformer. From the peak of the cross correlation, a time delay, $\Delta\tau$, due to the difference in arrival time between the two adjacent microphones is found. Then, using the assumption that waves in the vicinity of the microphones are locally planar and travelling at the speed of sound, c, a distance, $c \cdot \Delta\tau$, is found to form a right angle between the arrival path to the downstream microphone and the wavefront in contact with the upstream microphone. This creates a right triangle which can be used to solve for the angle of incidence, ψ, in terms of $c \cdot \Delta\tau$ and the interelement spacing along the array, d,

$$\psi = \cos^{-1}\left(\frac{c \cdot \Delta\tau}{d}\right). \tag{1}$$

The array offset angle, ϕ (shown in Fig. 5), is then directly computed from the difference in the microphone locations,

$$\phi = \tan^{-1}\left(\frac{\Delta x}{\Delta z}\right), \tag{2}$$

and then ϕ and ψ are used to compute the directivity of the sound in terms of the jet inlet angle,

$$\theta = 180° - (\psi + \phi). \tag{3}$$

Tracing the incident angle back to the nozzle lipline gives an apparent source region of the flow corresponding to the event. Each apparent source location and directivity angle found for each of the 1000 events are then compiled into normalized histograms, and the process repeated for each microphone pair in the array.

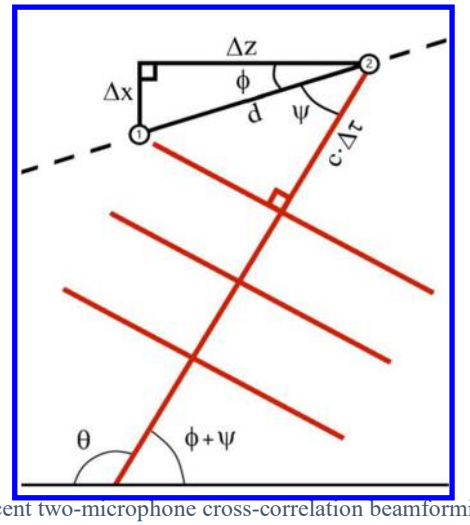

Figure 5. Schematic depicting the adjacent two-microphone cross-correlation beamforming method.

IV. Event-Based Beamforming Results

The event-based beamforming process described above has been applied to the F-35B, for engine conditions between 75% and 150% ETR, which have far-field derivative skewness values sufficient for the perception of continuous crackle at many angles.[24] Section IV.A presents normalized histograms of the propagation angle and apparent origin of the highest 1000 derivative events beamformed from microphone pairs along the ground array for 75% and 150% ETRs. Additional comparisons across all four engine conditions are made in Sec. IV.B.

A. Normalized Histograms

The occurrences of beamformed directivity angles are shown as normalized histograms for 75% and 150% ETR in Fig. 6. The abscissa is the z-coordinate of the upstream microphone along the array as pictured in Fig. 1 and the ordinate is the histogram bins (representing inlet angle in degrees). The colormap corresponds to the normalized histogram of angles for each microphone pair, where the histogram counts are divided by the total number of events. Probabilities below 0.05 are set to white to emphasize the dominant trends. There is a distinct separation in the peak of the distributions between 3-4 m along the array, where the directivity angle of the maximum derivative events changes from upstream ($\theta < 90°$) to the downstream direction. Based on recent spectral characterizations,[27,28] the upstream region is associated with broadband shock-associated noise (BBSAN), which is a dominant noise source in the forward direction. While fine-scale noise is also present in the forward direction, the absence of derivatives pointing directly to the sideline (where the BBSAN levels decrease and the fine-scale noise dominates) likely indicates that the high-derivative events in the forward direction are associated with BBSAN.[27]

Downstream locations beyond 3 m for 75% ETR and 4 m for 150% ETR all have angles greater than 90°, indicating downstream propagation from their apparent origin to the microphone array. For 75% ETR, propagation angles increase quickly at first, then nearly level off at the end of the microphone array, whereas for 150% ETR the propagation angles remain constant for about 8 m before increasing to the end of the array. This region of consistent propagation angle in the 150% ETR case is consistent with unidirectional Mach wave radiation,[33] stemming from a constant convective velocity over some extent of the plume. At the end of the microphone array, the propagation angles converge to $155°$ for 75% ETR and $150°$ for 150% ETR. These propagation angles along the microphone array when traced to the jet lipline yield an apparent origin of these top derivative events.

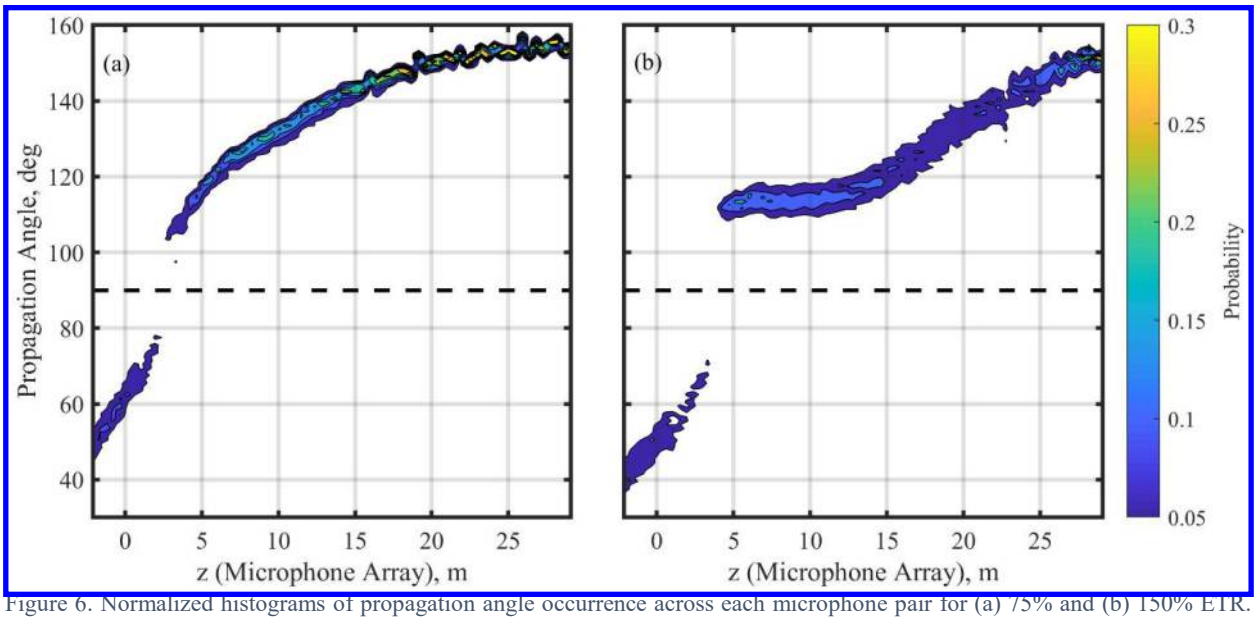

Figure 6. Normalized histograms of propagation angle occurrence across each microphone pair for (a) 75% and (b) 150% ETR. The dashed lines indicate 90°, where angles below propagate upstream to the microphone array and angles below propagate downstream.

The propagation angles in Fig. 6 have been used to produce ray-traced apparent origins for the high-derivative events at all four ETR of interest. The resulting normalized histograms for apparent origin along x = 0.5 m (approximately the nozzle lipline) are shown in Fig. 7 for 75% and 150% ETRs. The x-axis shows the location of the upstream microphone in each pair with the y-axis representing the apparent origin along the lipline. For 75% ETR in Fig. 7a, the top derivative events found at the farthest upstream microphones appear to originate from 3-5 m downstream, which corresponds to the angles with upstream propagation and the previously described BBSAN. Continuing down the microphone array, the effect of the discontinuity in the propagation angle at 3 m along the array is seen with the apparent origin suddenly shifting upstream along the lipline. The histograms with the least spread occur after this transition from 4-12 m downstream along the jet lipline and is localized 1-3 m along the jet lipline for 75% ETR. Downstream of this region, the mode of the apparent origins shifts downstream while the distribution broadens. In contrast, at 150% ETR, the farthest upstream region associated with upstream radiation and BBSAN occurs from 4-8 m along the lipline. The transition between upstream and downstream radiation occurs slightly farther downstream at 4 m and experiences a greater jump for 150% ETR. The densest grouping of apparent origins occurs from about 4.5-14 m along the array with apparent origins ranging from 4-9 m along the lipline. Downstream of this region, the mode for each microphone pair shifts slightly downstream until about 20 m where the now broad distribution begins to move back upstream along the lipline. This last result indicates that the events creating the largest derivatives present at the far aft portion of the microphone array at maximum afterburner do not originate from a corresponding far-aft position.

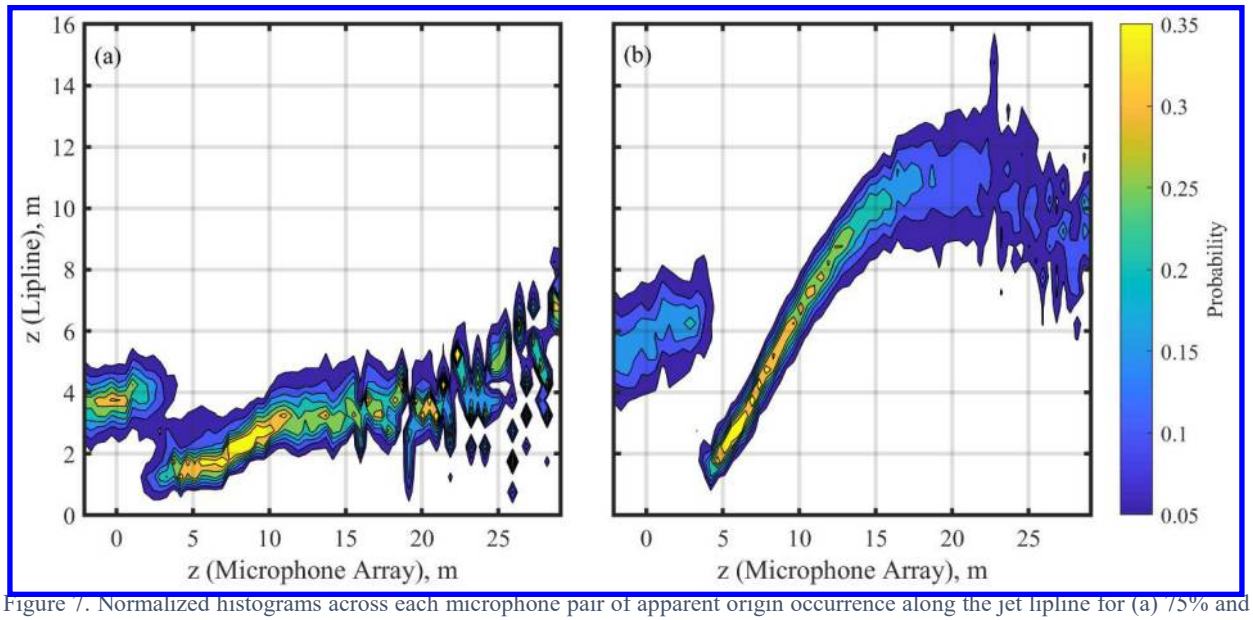

Figure 7. Normalized histograms across each microphone pair of apparent origin occurrence along the jet lipline for (a) 75% and (b) 150% ETR.

B. Normalized Histogram Mode Comparison Across ETR

By simplifying the results in Figs. 6 and 7, trends across ETR for propagation angle and apparent origin can be examined. Each histogram is reduced to its mode (with a 1° or 0.25 m resolution) and the results are shown in Fig. 8. While both the mode and mean show similar trends, the mode is used to better represent the abrupt transition in source location for upstream to downstream propagation. The inclusion of 100% and 130% ETRs demonstrate intermediate cases for the previously analyzed 75% and 150% ETRs.

While exhibiting similar features across engine conditions, notable differences exist. At the farthest upstream locations, the propagation angle decreases with increased engine condition making the apparent origin shift downstream. The amount of decreased angle or increased apparent origin varies along the array with the most notable change in angle occurring after transitioning from below to above 90° propagation at 3-4 m (see Fig. 8a). Higher engine conditions have a region with minimal change in propagation angle, which appears as the increasing lipline origin in Fig. 8b from 4-15 m. Above 75% ETR, an inflection point where the apparent origin along the lipline transitions from downstream to upstream progression is shown in Fig. 8b. This transition occurs at about 15 m for 100%, about 17 m for 130%, and 20 m for 150% ETR. Beyond this region for 100% ETR, propagation angles increase to be nearly identical to 75% ETR from 19 m to the end of the array. At 130% ETR, 27 m to the end of the array is nearly identical to lower engine conditions, and while 150% ETR does decrease, it does not match those of lower engine conditions. This trend at the end of the array is interesting to note as the derivative skewness values vary greatly in this region where propagation angles and apparent origins are similar.

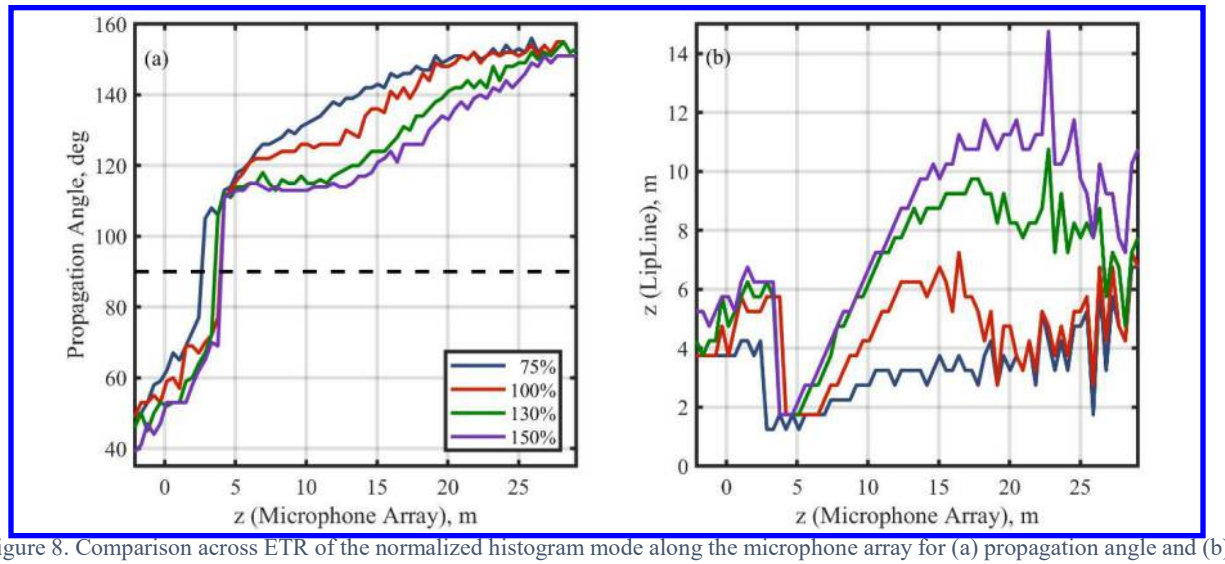

Figure 8. Comparison across ETR of the normalized histogram mode along the microphone array for (a) propagation angle and (b) apparent origin. Black dashed line in (a) indicates 90°, where angles below propagate upstream to the microphone array and angles below propagate downstream.

V. Analysis

Using the results of the event-based beamforming method implemented in this study, microphone pairs are sorted into groups using criteria suggested in Section V.A. Criteria used include the propagation angles found through the event-based beamforming, the measured dSk, and measured OASPL. The groupings are then assigned a color for distinction and examined via a graphical representation using the measurement geometry in Section V.B. Groups associated with crackle content are further discussed and analyzed in Section V.C, and a comparison with near-field acoustical holography previously performed on the same data set is given in Section V.D

A. Microphone Pair Groupings

Microphone pairs are placed into one of six groups that are defined using trends in the beamformed angle of the derivative events as well as the dSk and OASPL measured at the upstream microphone within the pair. These grouping criteria build upon the previously developed four groups used in Ref. 30 and are displayed in Table 1. The first criteria for categorizing the microphone pairs are whether or not the mode of the beamformed propagation angles are pointed upstream (<90°) or downstream (>90°) and by whether or not the directionality is changing along the array or is unidirectional (less than 2° changes compared to adjacent microphones pairs, denoted by <Δ2°). The second criteria is whether or not the dSk is greater or less than 3, indicating the presence of continuous crackle.[22] The final criteria for group distinction is whether or not the microphone pair is upstream, downstream, or in the vicinity of a peak in the OASPL along the array. The first peak is at about 10 m and the second peak is beyond 22 m along the array. Application of these criteria to the microphone pairs for the four engine conditions generates six distinct groups.

Table 1. Criteria for six groups used in Figs. 9 and 10. Angles indicate upstream (<90°), downstream (>90°), or unidirectional propagation (<Δ2°) from the jet lipline to microphone array. Derivative skewness (dSk) values are used to indicate whether continuous crackle is (>3) or is not (<3) present. Overall sound pressure level (OASPL) denotes whether the microphone pair is upstream, downstream, or in the vicinity of the first or second peak in the OASPL along the array.

Criteria	Group 1 (Blue)	Group 2 (Red)	Group 3 (Purple)	Group 4 (Green)	Group 5 (Yellow)	Group 6 (Orange)
Angle	< 90°	> 90°	< Δ2°	> 90°	> 90°	> 90°
dSk	< 3	< 3	> 3	> 3	> 3	< 3
OASPL	Upstream	Upstream	1st Peak	1st Peak	2nd Peak	Downstream

Groups, with their respective trend for each of the three criteria shown in Table 1, are numbered are numbered by their occurrence along the microphone array from upstream to downstream. Comparing across groups for the first criterion, only group 1 propagates upstream from the apparent origin to the array while groups 2-6 all exhibit downstream propagation. Group 3 is characterized by a minimal change in propagation angle across microphone pairs

indicating unidirectional radiation within the group. Groups 1, 2, and 6 have a dSk below the threshold of 3 while groups 3-5 all exceed a dSk of 3 indicating the presence of continuous crackle. The last criterion using relative location to OASPL peaks along the array primarily differentiates groups 3 and 4 near the first peak from group 5 at the second peak, with groups 1 and 2 occurring upstream of the first peak and group 6 downstream of the second peak at the end of the array.

The three criteria are plotted along the microphone array for 75%, 100%, 130%, and 150% ETR in Fig. 9. Engine conditions are noted by shape while colors signify the group classification as noted in Table 1. This allows for comparison of criteria across group and ETR. Propagation angle comparison across ETRs are presented in Section IV.B. The dSk is similar across all engine conditions up to 22 m along the array, where the dSk diverges with greater values at lower engine conditions. Previously-made spatial dSk maps from data collected at off-ground microphone arcs for the same F-35 measurement by Gee *et al.*[34] show dSk decreasing with downstream distance after peaking, as is seen with 150% ETR in Fig. 9b. Further investigation into this phenomenon should lend insight into understanding crackle, as it is curious that dSk increases with lower OASPL at lower engine conditions.

The general shape of the OASPL across the array in Fig. 9c is similar across engine conditions with the first, main peak at about 10 m and a second peak at about 22 m. Peak levels increase up to 130% ETR, then slightly decrease at 150% ETR. The first peak shifts slightly upstream and broadens with ETR, while the second peak occurs at the same location, but with a steeper roll off towards the end of the array at higher engine conditions. Though the levels plotted in Fig. 9 are directly computed from the data, the second peak in the OASPL is more pronounced when the levels are spatially normalized to a common reference distance, as seen in Ref. 30.

Groups 1, 2, 4, and 5 exist at all engine conditions. These correspond to groups previously described in analyzing the 75% ETR case in Ref. 30. Inclusion of higher engine conditions requires the addition of group 3, with its minimal change in propagation angle over space (see Fig. 9a) that first appears at 100% ETR. Group 6 emerges at the end of the array for 150% ETR where the dSk drops below 3. At lower conditions, the dSk value in this region is above 3, classifying it as part of group 5 instead of 6.

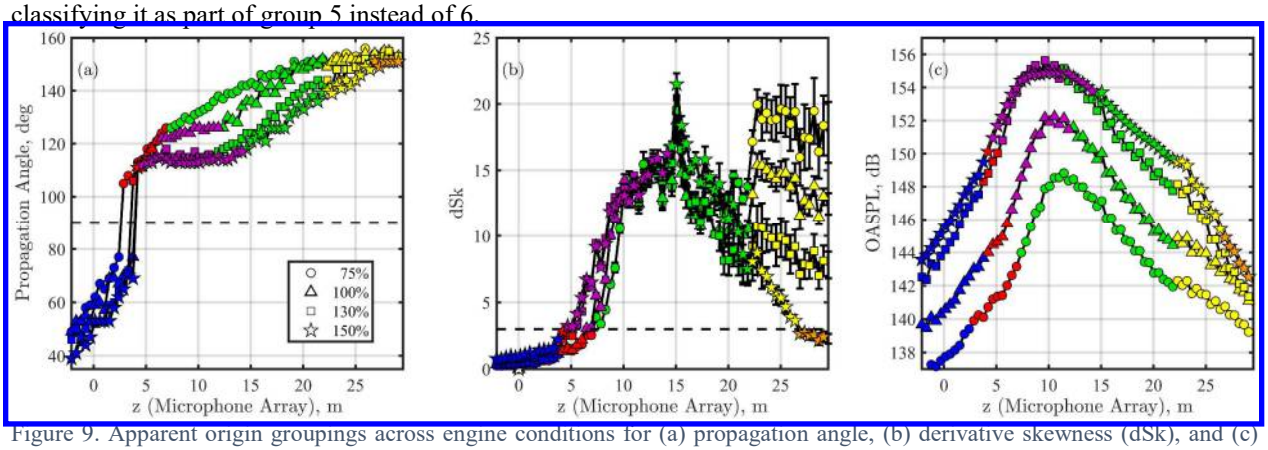

Figure 9. Apparent origin groupings across engine conditions for (a) propagation angle, (b) derivative skewness (dSk), and (c) overall sound pressure level (OASPL) along the microphone array with six distinct colored groupings. Engine conditions are noted by symbols as noted in the legend.

B. Colored Traced Origins

Groups defined in Section V.A are related to the propagation angles and apparent origins of the beamformed events. First, a graphical representation in Fig. 10 uses the mode of the traced angles from each microphone pair to draw a line from the array to the nozzle lipline. Fig. 10 shows these traced lines (color coded to represent their grouping) with a schematic of the F-35, the nozzle lipline, the approximate location of the shear layer, and the array location. Additionally, the ranges of the directivities and source locations for each engine condition are given in Tables 2 and 3, with rows representing different ETR conditions and columns indicating the angular or spatial ranges for a given group.

With increasing ETR, the apparent source locations of group 1 broadens slightly and shifts downstream. Group 2 remains closest to the nozzle with the least amount of variation of all the groups. First appearing at 100% ETR, group 3 has nearly the same upstream lipline location as subsequent ETR conditions with an expanded coverage as ETR increases. Group 4 covers a similar range while the entire span shifts downstream with increased ETR. Group 5 is broader than Group 4 and shifts slightly downstream with increasing ETR. However, rather than converging, the rays begin to cross over and appear to come from far upstream, overlapping with Group 4. Only appearing at 150% ETR, group 6 exemplifies this crossover behavior.

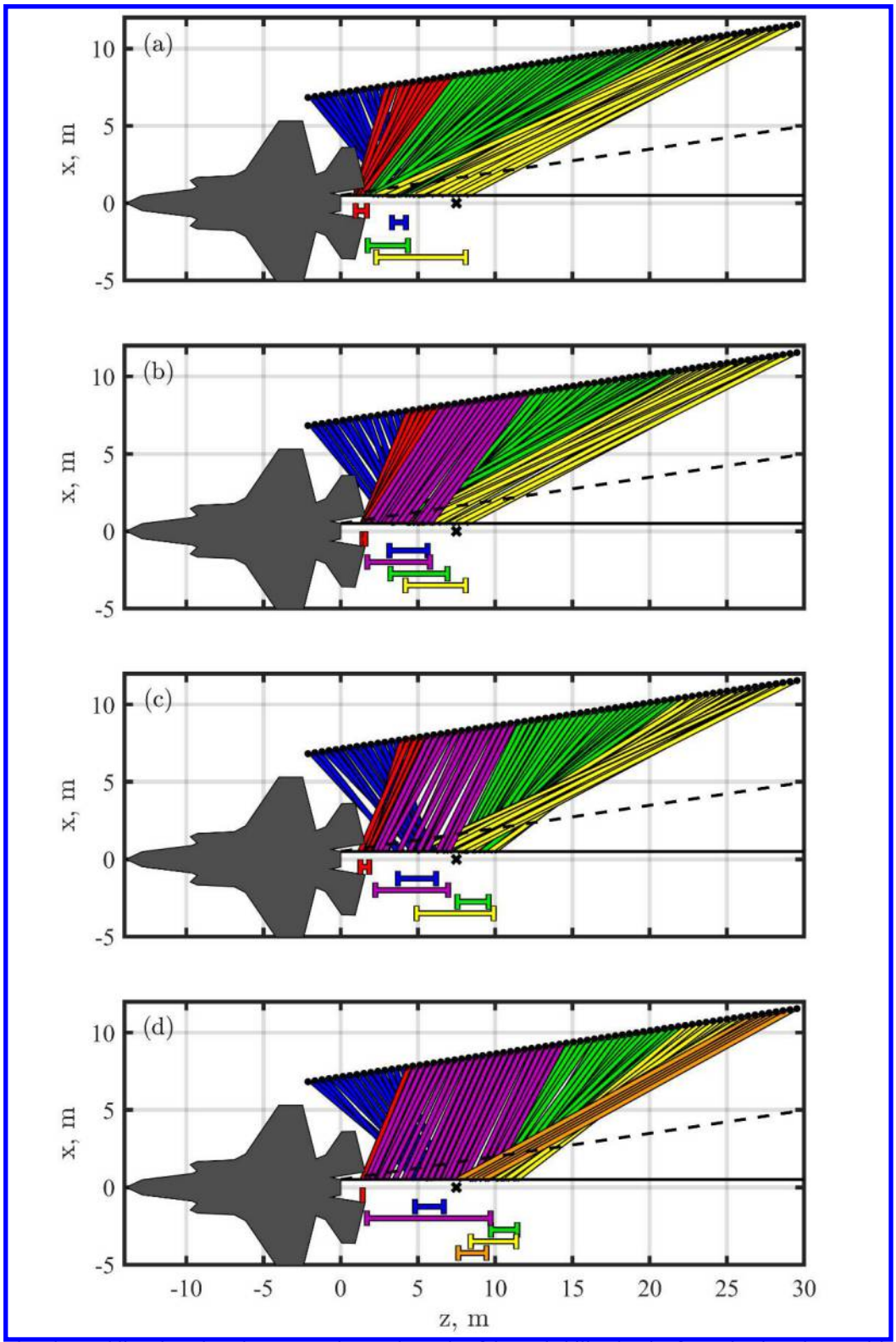

Figure 10. Colored traced lines based on the propagation angle mode of the probability density for each microphone pairing for (a) 75%, (b) 100%, (c) 130%, and (d) 150% ETR. The jet nozzle lipline and estimated shear layer are indicated respectively by black solid and dashed lines, while a black "X" represents the MARP.

Table 2. Apparent origin ranges along the jet lipline for the groupings across ETR. Groupings that do not apply to a particular engine condition are noted with a dash (-). Values are associated with the modes of the probability densities for each microphone pair.

ETR	Group 1	Group 2	Group 3	Group 4	Group 5	Group 6
75%	3.3 – 4.2 m	1.0 – 1.7 m	-	1.8 – 4.4 m	2.3 – 8.1 m	-
100%	3.2 – 5.6 m	1.4 – 1.6 m	1.7 – 5.8 m	3.2 – 6.9 m	4.2 – 8.1 m	-
130%	3.7 – 6.2 m	1.3 – 1.8 m	2.2 – 7.0 m	7.6 – 9.6 m	4.9 – 9.9 m	-
150%	4.8 – 6.7 m	1.4 m	1.7 – 9.7 m	9.7 – 11.4 m	8.4 – 11.4 m	7.6 – 9.4 m

Table 3. Propagation angle ranges for the groupings across ETR. Values are associated with the modes of the probability densities for each microphone pair.

ETR	Group 1	Group 2	Group 3	Group 4	Group 5	Group 6
75%	49 – 77 º	105 – 126 º	-	126 – 152 º	150 – 156 º	-
100%	49 – 77 º	111 – 121 º	122 – 126 º	126 – 152 º	149 – 155 º	-
130%	45 – 72 º	106 – 114 º	113 – 118 º	115 – 144 º	142 – 155 º	-
150%	39 – 70 º	111 º	112 – 117 º	118 – 139 º	139 – 149 º	149 – 151 º

C. Crackle-related Groups

Groups 3, 4, and 5, all exceed the criterion developed in Ref. [22] for the perception of "continuous crackle" at the array. As shown in Fig. 9c, groups 3 and 4 have the highest OASPL values across all ETR. The dSk is highest for group 5 at 75% ETR, decreases at 100% ETR to a similar value across all three groups, and as engine condition is increased, the dSk in group 5 decreases. Propagation angles increase from group 3 to 5 for each ETR (see Fig. 9a and Table 3). For each group, there is a slight decrease in propagation angle with increasing ETR. Group 3 only decreases slightly in propagation angle after 100% ETR and is essentially the same for 130% and 150% ETR; group 4 has the same directivity for 75% and 100% ETR, then decreases by about 10º for 130% and 150% ETR; and group 5 remains nearly constant across all engine conditions with only a slight decrease at higher powers. When traced back to the nozzle lipline in Fig. 10, it is seen that the three crackle-related groups have different corresponding source regions and directivities, all of which cover the aft radiation portion, in the direction of maximum radiation. Though this is expected simply because the levels are high in this region, comparison of the behavior between these groups as well as previous inverse methods applied to the same aircraft yield additional insight into the jet noise field.

D. Near-field Acoustical Holography Comparison

The beamforming of the top derivative events shown in this paper is fundamentally different than other inverse methods that have been applied to this data set. An ongoing research topic is the use of near-field acoustical holography (NAH)[29,35,36] to reconstruct the entire acoustic field using the same measurement array discussed in this work. The NAH method creates an equivalent wave model for cylindrically spreading waves originating at the jet centerline (as well as an image jet centerline below the ground to model the ground reflection) and fits that model to the frequency-domain data along the measurement array. With the use of frequency-domain data, it is inherently a representation of the time-averaged energy of the field, as opposed to the current method, which looks at the histogram of beamformed results of multiple small portions of the waveform.

Where the cross correlation is a broadband calculation, the NAH method is performed one frequency at a time and has frequency limitations because of the physical size and density of the array. The OASPL band-limited to the range of frequencies where NAH was implemented (30-400 Hz) along the array and the reconstructed OASPL along the lipline using the NAH method is pictured in Fig. 11. The horizontal axis is the downstream position along the nozzle lipline or microphone array and the vertical axis is OASPL. Due to band-limiting, the levels drop significantly for the farthest upstream microphones in Fig. 11a, as the peak in the spectra from BBSAN is greater than 400 Hz.[27,28] In addition, the peak level decreases, shifts downstream for all ETR to about 12-13 m, and broadens. The OASPL peak is farther downstream at the array than lipline (as expected for directional radiation), but unlike at the microphone array, secondary peaks in the OASPL at the lipline in Fig. 11b are much weaker. Also, the peak reconstructed OASPL at the lipline shifts farther downstream with increasing ETR.

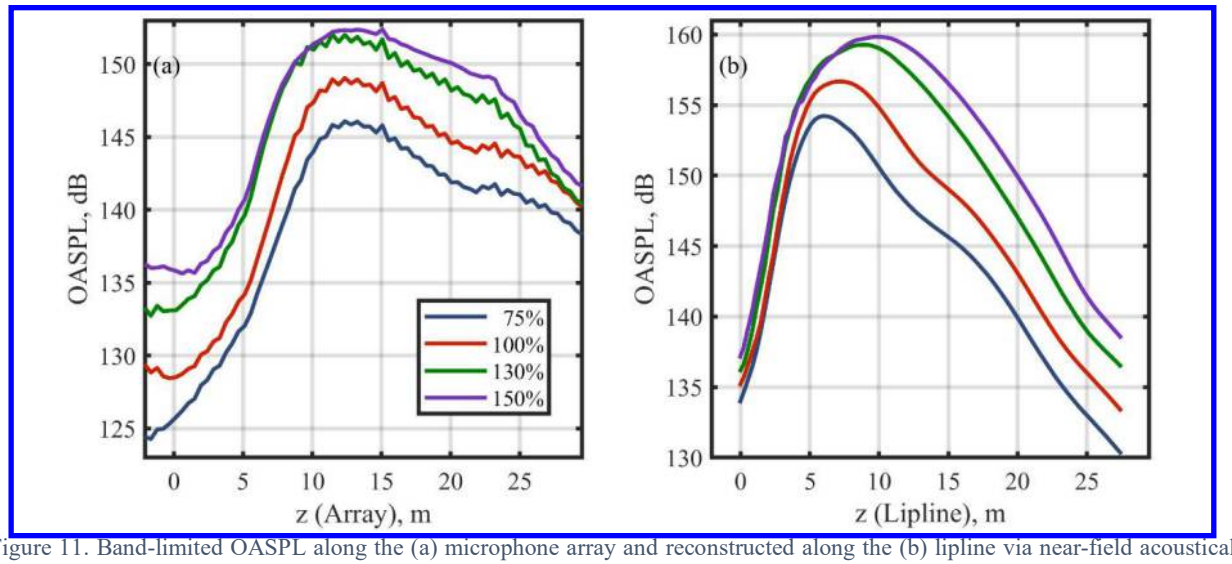

Figure 11. Band-limited OASPL along the (a) microphone array and reconstructed along the (b) lipline via near-field acoustical holography.

For 75% ETR, the reconstructed OASPL peak along the lipline in Fig. 11b occurs at 6.0 m with a 3 dB down region from 4.0-9.5 m. Comparing this region to Fig. 10a, the high-derivative events that appear to originate from 4.0-9.5 m along the lipline beam outward primarily to microphones downstream of 19 m with a few tracing upstream to 2-4 m. These microphones are sorted into group 4, 5 and 1. Of all of the microphone pairs that are in groups 3, 4, and 5, there are almost no derivative events which originate from 7.5-9.5 m along the lipline, even though the 3 dB down region from the NAH reconstructions extends to 9.5 m and contains significant energy beyond. Group 4, which includes the main OASPL peak along the array for both the broadband and band-limited cases and high dSk values, appears to originate primarily from 1.8-4.4 m along the lipline which is upstream of the 3 dB down region of the NAH reconstructions. Group 5 includes the highest dSk values along the array, the second peak in the OASPL, and apparent origin from 2.3-7.5 m, which ovelaps with the upstream half of the 3 dB down region of the NAH reconstructions. Group 1 is associated with the BBSAN, which in this measurement has a low dSk value. It appears that the origin of waveforms in the field with elevated dSk (to the point of the perception of at least "continuous crackle") is upstream of the origin of the time-averaged energy in the field estimated by NAH.

On the other hand, at 150% ETR the apparent source locations for the crackle-related events seem to agree with the NAH results. The reconstructed OASPL peak along the lipline for 150% ETR in Fig. 11b occurs approximately at 10 m with a 3 dB down region ranging from 5.4-14.8 m along the lipline. Comparing this region to Fig. 10a, the high-derivative events that appear to originate from this region along the lipline correspond to all of groups 4, 5, and 6 with large portions of groups 3 and 1 included as well. Groups 3 and 4 have similar dSk values but group 3 has larger OASPL value, and of the crackle-related groups (3-5) group 5 has the lowest dSk and OASPL values for this engine condition. Group 4 traces right back to the NAH reconstructed peak and a little after, while the region along the lipline that group 5 traces to straddles the peak. Group 3, however, has unidirectional radiation spanning lipline region starting at 1.7 m and ending at 9.7 m, right before the peak of the NAH reconstruction. The portion of group 3 that falls outside of the 3 dB down region along the lipline corresponds to band-limited levels that are 10 dB lower than the broadband levels shown in Fig. 9c. The bandlimited OASPL peak along the array (~12-15 m, which belongs to groups 3 and 4) traces back to the reconstructed peak along the lipline (10 m) as expected, whereas the broadband OASPL peak along the array (~10-12 m) traces upstream of the reconstructed OASPL peak along the lipline (10 m) according to the event-based beamforming in this paper.

The majority of the microphone pairs in crackle-related groups at 150% ETR appear to originate within the maximum time-averaged energy region along the lipline identified by NAH. This is corroborated by the far-field directivity shown by James *et al*.,[24] which are calculated from the OASPL measured at far-field arcs. At 150% ETR, group 4 shares the same directivities as the far-field measurements, while group 5 has higher and group 3 has slightly lower directivities. Group 4 also agrees with far-field dSk trends at 150% ETR.[34] For 75% ETR, group 4 again agrees with the far-field OASPL directivities, while group 5, which has higher dSk, has higher directivities. These differing directivities seen for the event-based beamformed groups may be related to the multiple spatiospectral lobes observed in several works,[25,26,29,35,36] which in turn may be related to different mechanisms by which the turbulence in the jet flow radiates to the far field.[29,37] For example, the unidirectional directivity of group 3 is consistent with of the

description of Mach wave radiation.[33] As the different groups had varying dSk values, it is plausible that some source radiation mechanisms may generate high dSk more readily than others. Further analysis into how these groups are translated into the far field and if they correspond to different source mechanisms in the plume is needed to understand the relative importance of source generation of high dSk versus the role of nonlinear propagation to increase the dSk to the percept of crackle in the far field.

VI. Conclusion

This paper has identified regions along the nozzle lipline of a military aircraft that correspond to higher crackle percept in the field[22,23] by an event-based beamforming method. Small windows of the waveform around 1000 of the highest derivative values are chosen as events in the beamforming process. Microphone pairs are grouped together according to propagation angle from the event-based beamforming and measured dSk and OASPL trends. Six distinct groupings have been defined, with particular interest given to those with dSk values greater than 3 (groups 3-5). These three crackle-related groups propagate downstream but have differing source locations and directivities. Group 3 has unidirectional radiation, consistent with the description of Mach wave radiation upstream of the potential core.[33] Groups 3 and 4 correspond to the main peak in the OASPL along the array while group 5 corresponds to a second peak towards the end of the array. The differences between groups 3, 4 and 5 appear to be similar to differences in spatiospectral lobes previously observed in the F-35 field.[25,26,29] Comparisons with NAH results indicate that at 75% ETR, the apparent origin of crackle-related events is slightly upstream of the maximum time-averaged energy region defined by NAH, whereas at 150% ETR, the apparent origin of the top derivative events seems to agree with the maximum energy region defined by NAH. The absence of group 3 from the 75% ETR case may factor into this observed difference. Overall, beamforming of crackle-related events has shown that the source mechanisms responsible for the percept of crackle in the field may not necessarily be the same as the source mechanisms responsible for producing the majority of the sound energy of the jet.

Acknowledgments

The authors gratefully acknowledge funding for the measurements, provided through the F-35 Program Office and Air Force Research Laboratory. (Distribution A: Approved for public release; distribution unlimited. F-35 PAO Cleared 04/24/2019; JSF19-326) This research was funded under an Air Force Research Laboratory SBIR program. (DFARS 252.227-7018 (JUNE 1995)); Contract Number: FA8650-16-C-6717; Contractor Name & Address: Blue Ridge Research and Consulting, LLC, 29 N Market St, Suite 700; Asheville, NC; Expiration of SBIR Data Rights: Expires five years after completion of project work for this or any follow-on SBIR contract, whichever is later. (Subject to SBA SBIR Directive of September 24, 2002). The Government's rights to use, modify, reproduce, release, perform, display, or disclose technical data or computer software marked with this legend are restricted during the period shown as provided in paragraph (b)(4) of the Rights in Noncommercial Technical Data and Computer Software-Small Business Innovation Research (SBIR) Program clause contained in the above identified contract. No restrictions apply after the expiration date shown above. Any reproduction of technical data, computer software, or portions thereof marked with this legend must also reproduce the markings.

References

[1] Ffowcs Williams, J. E., Simson, J., and Virchis, V. J., " 'Crackle': An annoying component of jet noise," *Journal of Fluid Mechanics*, Vol. 71, No. 2, 1975, pp. 251–271. DOI:10.1017/S0022112075002558

[2] Krothapalli, A., Venkatakrishnan, L., and Lourenco, L., "Crackle: A dominant component of supersonic jet mixing noise," AIAA Paper 2000-2024, June 2000. DOI:10.2514/6.2000-2024

[3] Gee, K. L., Gabrielson, T. B., Atchley, A. A., and Sparrow, V. W., "Preliminary analysis of nonlinearity in military jet aircraft noise propagation," *AIAA Journal*, Vol. 43, No. 6, 2005 pp. 1398–1401. DOI:10.2514/1.10155

[4] Gee, K. L., Sparrow, V. W., James, M. M., Downing, J. M., Hobs, C. M., Gabrielson, T. B., and Atchley, A. A., "The role of nonlinear effects in the propagation of noise from high power aircraft," *Journal of the Acoustical Society of America*, Vol. 123, No. 6, 2008, pp. 4082–4093. DOI:10.1121/1.2903871

[5] Gee, K. L., Downing, J. M., James, M. M., McKinley, R. C., McKinley, R. L., Neilsen, T. B., and Wall, A. T., "Nonlinear evolution of noise from a military aircraft during ground run-up," AIAA Paper 2012-2258, June 2012. DOI:10:2514/6.2012-2258

[6] Gee, K. L., Neilsen, T. B., Muhlestein, M. B., Wall, A. T., Downing, J. M., James, M. M., and McKinley, R. L., "On the evolution of crackle in jet noise from high-performance engines," AIAA Paper 2013-2190, June 2013. DOI:10:2514/6.2013-2190

[7] Baars, W. J., Tinney, C. E., Wochner, M. S., and Hamilton, M. F., "On cumulative nonlinear acoustic waveform distortions from high-speed jets," *Journal of Fluid Mechanics*, Vol. 749, 2014, pp. 331–366. DOI:10.1017/jfm.2014.228

[8] Daniel, K., Mayo Jr., D., Lowe, K. T., and Ng, W. F., "Experimental investigation of the pressure field of a heated supersonic jet with a centered total temperature non-uniformity," AIAA Paper, 2018-3145, June 2018. DOI:10.25/6.2018-3145
[9] Martens, S., Spyropoulos, J. T., and Nagel, Z., "The effect of chevrons on crackle—Engine and scale model results," in ASME Turbo Expo 2011 (2011). DOI:10.1115/GT2011-46417
[10] Nichols, J. W., Lele, S. K., Ham, F. E., Martens, S., and Spyropoulos, J. T., "Crackle noise in heated supersonic jets," *Journal of Engineering for Gas Turbines and Power*, Vol. 135, No. 5, 051202, April 2013. DOI:10.1115/1.4007867
[11] Nichols J. W., Lele, S. K., and Spyropoulos, J. T., "The source of crackle noise in heated supersonic jets," AIAA Paper 2013-2197, Vol. 135, No. 5, June 2013. DOI:10.2514/6.2013-2197
[12] Buchta, D. A., Anderson, A. T., and Freund, J. B., "Near-field shocks radiated by high-speed free-shear flow turbulence," AIAA Paper 2014-3201, June 2014. DOI:10.2514/6.2014-3201
[13] Pineau, P., and Bogey, C., "Study of the generation of shocks by high-speed jets using conditional averaging," AIAA Paper 2018-3305, June 2018. DOI:10.2514/6.2018-3305
[14] Fievet, R., Tinney, C. E., and Baars, W. J., "Acoustic waveforms produced by a laboratory scale supersonic jet," AIAA Paper 2014-2906, June 2014. DOI:10.2514/6.2014-2906
[15] Murray, N.E., and Lyons, G.W., "On the convection velocity of source events related to supersonic jet crackle," *Journal of Fluid Mechanics*, Vol. 793, 2016, pp. 477-503. DOI:10.1017/jfm.2016.127
[16] Veltin, J., Day, B. J. and McLaughlin, D. K., "Correlation of flowfield and acoustic field measurements in high-speed jets," *AIAA Journal*, Vol. 49, pp. No. 1, pp. 150-163. DOI:10.2514/1.J050583
[17] Tam, C. K. W., Spyropoulos, J. T., Aubert, A. C., and Powers, R. W., "Crackle in the noise of high-performance aircraft," AIAA Paper 2018-3306, June 2018. DOI:10.2514/6.2018-3306
[18] Mora, P., Heeb, N., Kastner, J., Gutmark, E. J., and Kailasanath, K., "Effect of heat on the pressure skewness and kurtosis in supersonic jets," *AIAA Journal*, Vol. 52, No. 4, 2014, pp 777–787. DOI:10.2514/1.J052612
[19] Chen, S., Gojon, R., and Mihaescu, M, "High-temperature effects on aerodynamic and acoustics characteristics of a rectangular supersonic jet," AIAA Paper 2018-3303, June 2018. DOI:10.2514/6.2018-3303
[20] Gee, K. L., Sparrow, V. W., Atchley, A., and Gabrielson, T. B., "On the perception of crackle in high-amplitude jet noise," *AIAA Journal*, Vol. 45, No. 3, 2007, pp. 593-598. DOI:10.2514/1.26484
[21] Swift, S. H., Gee, K. L., Neilsen, T. B., "Testing two crackle criteria using modified jet noise waveforms," *Journal of the Acoustical Society of America*, Vol. 141, No. 6, 2017, pp. EL549-EL554. DOI:10.1121/1.4984819
[22] Gee, K. L., Russavage, P. B., Neilsen, T. B., Swift, S. H., and Vaughn, A. B., "Subjective rating of the jet noise crackle percept," *Journal of the Acoustical Society of America*, Vol. 144, No. 1, 2018, pp. EL40-EL45. DOI:10.1121/1.5046094
[23] Russavage, P. B., Neilsen, T. B., Gee, K. L., and Swift, S. H., "Rating the perception of jet noise crackle," Proc. Mtgs. Acoust. Vol. 33, No. 1, p. 040001. (2018). DOI:10.1121/2.0000821
[24] James, M. M., Salton, A. R., Downing, J. M., Gee, K. L., Neilsen, T. B., Reichman, B. O., McKinley, R. L., Wall, A. T., and Gallagher, H. L. "Acoustic emissions from F-35B aircraft during ground run-up," AIAA Paper 2015-2375, June 2015. DOI:10.2514/6.2015-2375
[25] Wall, A. T., Leete, K. M., Gee, K. L., Neilsen, T. B., James, M. M., and McKinley, R. L, "Preliminary investigation of multilobe fighter jet noise sources using acoustical holography," AIAA Paper 2017-3520, June 2017. DOI:10.2514/6.2017-3520
[26] Swift, S. H., Gee, K. L., Neilsen, T. B., Wall, A. T., Downing, J. M., and James, M. M., "Spatiotemporal correlation analysis of jet noise from a round-nozzle supersonic aircraft," AIAA Paper 2018-3938, June 2018. DOI:10.2514/6.2018-3938
[27] Neilsen, T. B., Vaughn, A. B., Gee, K. L., Swift, S. H., Wall, A. T., Downing, J. M. and James, M. M., "Inclusion of broadband shock-associated noise in spectral decomposition of noise from high-performance military aircraft," AIAA Paper 2018-3146, June 2018. DOI:10.2514/2018-3146
[28] Vaughn, A. B., Neilsen, T. B., Gee, K. L., Wall, A. T., Downing, J. M. and James, M. M., "Broadband shock-associated noise from a high-performance military aircraft," *Journal of the Acoustical Society of America*, Vol. 144, No. 3, 2018, pp. EL242-247. DOI:10.1121/1.5055392
[29] Leete, K. M., Wall, A. T., Gee, K. L., Neilsen, T. B., James, M. M., and Downing, J. M, "Dependence of high-performance military aircraft noise on frequency and engine power," AIAA Paper 2018-2826, June 2018. DOI:10.2514/6.2018-2826
[30] Vaughn, A. B., Gee, K. L., Swift. S. H., Wall, A. T., Downing, J. M., and James, M. M., "Beamforming of supersonic jet noise for crackle-related events," Proc. Mtgs. Acoust. Vol. 35, No. 1, p. 040003. (2018). DOI:10.1121/2.0000998
[31] Schlinker, R. H., Liljenberg, S. A., Polak, D. R., Post, K. A., Chipman, C. T., and Stern, A. M., "Supersonic jet noise source characteristics & propagation: Engine and model scale," AIAA Paper 2007-3623, June 2007. DOI:10.2514/6.2007-3623
[32] Laufer, J., Schlinker, R., and Kaplan, R. E., "Experiments on supersonic jet noise," *AIAA Journal* Vol. 14, No. 4, April 1976. DOI:10.2514/3.61388
[33] Murray, N. E., and Lyons, G. W., "On the convection velocity of source events related to supersonic jet crackle," *Journal of Fluid Mechanics,* Vol. 293, 2016, pp. 477-503. DOI:10.1017/jfm.2016.127
[34] Gee, K. L., Neilsen, T. B., Wall, A. T., Downing, J. M., James, M. M., and McKinley, R. L., "Propagation of crackle-containing jet noise from high-performance engines," *Noise Control Engineering Journal*, Vol. 64, No. 1, 2016, pp. 1-12. DOI:10.3397/1/376354
[35] Wall, A. T., Gee, K. L., Neilsen, T. B., "Multisource statistically optimized near-field acoustical holography," *Journal of the Acoustical Society of America*, Vol. 137, No. 2, 2015, pp. 963-975. DOI:10.1121/1.4906585

[36] Wall, A. T., Gee, K. L., Neilsen, T. B., McKinley, R. L., and James, M. M., "Military jet noise source imaging using multisource statistically optimized near-field acoustical holography," *Journal of the Acoustical Society of America*, Vol. 139, No. 4, 2016, pp. 1938-1950. DOI:10.1121/1.4945719

[37] Liu, J., Corrigan, A., Kailasanath, K., and Taylor, B., "Impact of the specific heat ratio on noise generation in a high-temperature supersonic jet," AIAA Paper 2016-2125, June 2016. DOI: 10.2514/2016-2125